Uncertainty Analysis of Air Radiation for Lunar Return Shock Layers

Bil Kleb[*] and Christopher O. Johnston[†]

By leveraging a new uncertainty markup technique, two risk analysis methods are used to compute the uncertainty of lunar-return shock layer radiation predicted by the High-temperature Aerothermodynamic Radiation Algorithm (HARA). The effects of epistemic uncertainty, or uncertainty due to a lack of knowledge, is considered for the following modeling parameters: atomic line oscillator strengths, atomic line Stark broadening widths, atomic photoionization cross sections, negative ion photodetachment cross sections, molecular bands oscillator strengths, and electron impact excitation rates.

First, a simplified shock layer problem consisting of two constant-property equilibrium layers is considered. The results of this simplified problem show that the atomic nitrogen oscillator strengths and Stark broadening widths in both the vacuum ultraviolet and infrared spectral regions, along with the negative ion continuum, are the dominant uncertainty contributors. Next, three variable property stagnation-line shock layer cases are analyzed: a typical lunar return case and two Fire II cases. For the near-equilibrium lunar return and Fire 1643-second cases, the resulting uncertainties are very similar to the simplified case. Conversely, the relatively nonequilibrium 1636-second case shows significantly larger influence from electron impact excitation rates of both atoms and molecules. For all cases, the total uncertainty in radiative heat flux to the wall due to epistemic uncertainty in modeling parameters is $\pm 30\%$ as opposed to the erroneously-small uncertainty levels ($\pm 6\%$) found when treating model parameter uncertainties as aleatory (due to chance) instead of epistemic (due to lack of knowledge).

I. Nomenclature

$\Delta\lambda_{S,0}$	Stark broadening width at 10,000 K and 10^{16} cm^{-3} electron number density
$\lambda_{CL,mult}$	Atomic multiplet centerline wavelength (nm)
ν	Photon frequency (eV)
σ	Statistical standard deviation
σ^-	Negative ion continuum cross section
σ_{bf}	Photoionization cross section
$c_i^{(k)}$	Cauchy-distributed value of i-th parameter, k-th sample
$e^{(k)}$	Scaled difference for k-th sample
f	Generic function
f_{ij}	Oscillator strength
h	Planck constant
I	Radiation intensity ($W/cm^2/sr$)
K_{el}	Electron-impact excitation rate
q_r	Radiative heat flux directed toward the wall (W/cm^2)
r_i	Uniformly-distributed random number on $(0,1)$ for i-th parameter
s_i	Sensitivity derivative of input parameter i
x_i	Input parameter i
y	Generic output value

---

[*]Aerospace Engineer, Aerothermodynamics Branch, Research Technology Directorate, lifetime AIAA member.
[†]Aerospace Engineer, Aerothermodynamics Branch, Research Technology Directorate, AIAA member.

II.   Introduction

The design of the thermal protection system (TPS) for NASA's lunar return capable Orion vehicle (also referred to as CEV) requires the accurate prediction of the shock layer radiative heating. Preliminary studies have shown that the radiative heating rate may be equal to or greater than the convective heating rate at peak heating conditions.[1] The High-temperature Air Radiation Algorithm (HARA) was recently developed at NASA Langley Research Center to provide these radiative heating predictions. The results of this code have been compared with the Fire II and Apollo 4 flight data,[2,3] as well as the recent Electric-Arc Shock Tube (EAST) measurements.[4,5] These comparisons have indicated a reasonable agreement between measurements and HARA predictions for the wavelength ranges measured, which were limited to wavelengths above 200 nm. The lack of data below 200 nm (the vacuum ultraviolet (VUV)) prevents the the validation of radiation models, such as the HARA code, in this wavelength range. This lack of experimental validation must be addressed since the VUV may contribute up to half of the total radiative flux for Orion.[1] An alternative to validating HARA with experimental data is to examine the accuracy (or uncertainty) of the physical parameters applied by HARA (which themselves are obtained from experiments) and determine their influence on the predicted radiative flux. The absence of VUV experimental data motivates this uncertainty analysis approach, which will also be valuable for rationalizing the minor disagreements between HARA and the non-VUV measurements cited previously as well as for quantifying the total radiative heating prediction uncertainty for Orion TPS design.

The following three sections describe the radiation modeling, the uncertainties considered, and the uncertainty analysis techniques. These sections are followed by results for a simplified shock layer problem problem, which considers the radiation emitted from two constant property layers of equilibrium air. This conceptually simple problem is relevant to the mostly equilibrium shock layers present at peak-heating lunar return conditions. Following the study of this simplified case are the analyses of three shock layer cases: a case representative of an Orion shock layer at peak heating and the Fire II 1636- and 1643-second trajectory point cases.

III.   Radiation Modeling

The HARA radiation model applied in the present study is discussed in detail by Johnston[2] and Johnston et al.[6,7] This model is based on a set of atomic levels and lines obtained from the National Institute of Standards and Technology (NIST)[8] and Opacity Project databases.[9] The atomic bound-free model is composed of cross sections from the Opacity project's online TOPbase,[10] which were curve fit to a convenient form by Johnston.[2] The molecular band systems are treated with the computationally efficient smeared-rotational band (SRB) model.[11] This approximate molecular model is accurate for the present lunar return applications because the emitting molecular bands are optically-thin.[12] The SRB model has also been shown to be sufficient for modeling strongly absorbing VUV band systems.[6] The non-Boltzmann modeling of the atomic and molecular electronic states is based on a set of electron-impact excitation rates compiled from the literature and presented in detail by Johnston.[2,7] Following the work of Park,[13] the quasi-steady state assumption is made when solving the Master Equation for the atomic and molecular electronic state populations.

IV.   Radiation Modeling Uncertainties

The following subsections describe the parameter uncertainties chosen for the present analysis. A total of 3627 individual uncertainty values were treated in this work.

A.   Atomic Lines

The atomic line model applied in HARA is discussed in detail by Johnston et al.[6] A brief review of this model, focused on the model uncertainty, is provided here. For the strongest lines of nitrogen and oxygen, the available data for oscillator strengths and Stark broadening widths were assessed by Johnston et al.[6] and uncertainty values were proposed. These uncertainties, for the oscillator strength (f_{ij}) and Stark broadening width ($\Delta\lambda_{S,0}$), are listed in Tables 1 and 2 for the strongest nitrogen and oxygen line multiplets. The choice of these uncertainties will be discussed in the following paragraphs.

American Institute of Aeronautics and Astronautics

For lines not listed in Tables 1 and 2, the f_{ij} uncertainties proposed by Wiese et al.[14] were applied for the NIST lines, and an uncertainty of $\pm 30\%$ was assumed for the additional Opacity Project lines.[9] The $\Delta\lambda_{S,0}$ uncertainties for lines not listed in Tables 1 and 2 were assumed equal to $\pm 50\%$ if the $\Delta\lambda_{S,0}$ value was taken from Griem[15] or Wilson and Nicolet.[16] Otherwise, the $\Delta\lambda_{S,0}$ value was obtained from an approximate correlation[6] and the $\Delta\lambda_{S,0}$ uncertainty was set to $\pm 100\%$.

Table 1: Strongest nitrogen line multiplets.

multiplet number	Wiese ID[*]	$h\nu$ (eV)	$\lambda_{CL,mult}$ (nm)	$\pm f_{ij}$ (%)	$\pm\Delta\lambda_{S,0}$ (%)
1	24	11.61	106.80	75	75
2	23	11.29	109.77	75	75
3	19	10.62	116.79	50	40
4	17	10.53	117.69	50	40
5	39	10.42	118.91	75	75
6	38	10.41	119.10	75	75
7	1	10.33	120.00	20	50
8	37	10.12	122.52	75	75
9	16	9.972	124.32	20	100
10	35	9.459	131.07	60	30
11	32	9.396	131.95	20	30
12	30	8.781	141.19	20	100
13	15	8.302	149.33	10	30
14	29	7.110	174.36	20	50
15	48	1.663	745.42	10	30
16	47	1.509	821.41	10	30
17	52	1.438	861.98	10	30
18	46	1.426	869.40	15	30
19	65	1.369	905.24	25	30
20	127	1.369	905.01	15	30
21	126	1.347	919.82	50	100
22	51	1.319	939.79	25	50
23	72	1.260	983.33	15	50
24	70	1.241	998.70	25	100
25	71	1.240	999.10	75	100
26	69	1.225	1011.7	10	50
27	80	1.158	1070.0	75	75
28	81	1.177	1052.6	10	75
29	68	1.098	1128.9	15	75
30	61	1.068	1160.0	25	100
31	100	1.029	1204.4	10	100
32	99	0.994	1246.9	15	100
33	114	0.910	1362.0	10	100

[*] Multiplet number listed by Wiese et al.[14]

Table 2: Strongest oxygen line multiplets.

multiplet number	Wiese ID[*]	$h\nu$ (eV)	$\lambda_{CL,mult}$ (nm)	$\pm f_{ij}$ (%)	$\pm\Delta\lambda_{S,0}$ (%)
1	2	9.51	130.35	3	50
2	56	1.59	777.55	3	50
3	60	1.47	844.88	10	50
4	64	1.34	926.64	3	50
5	78	1.09	1128.7	3	50

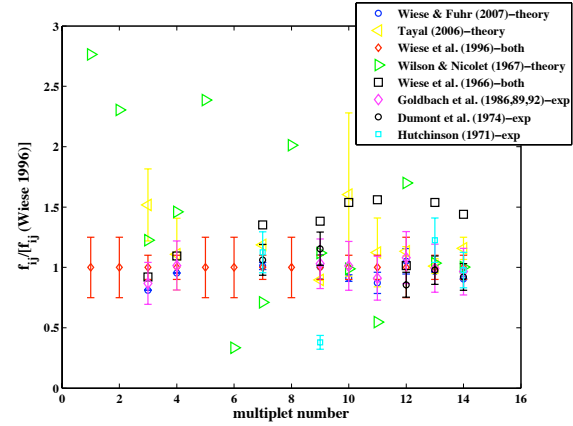[*] Multiplet number listed by Wiese et al.[14]

Figure 1: Predicted and measured nitrogen multiplet oscillator strengths, normalized by the Wiese et al.[14] values, for the first 14 multiplets of Table 1.
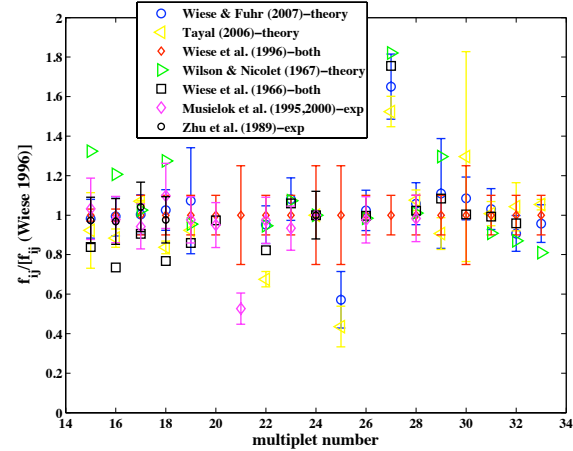

Figure 2: Predicted and measured nitrogen multiplet oscillator strengths, normalized by the Wiese et al.[14] values, for multiplets 15–33 of Table 1.
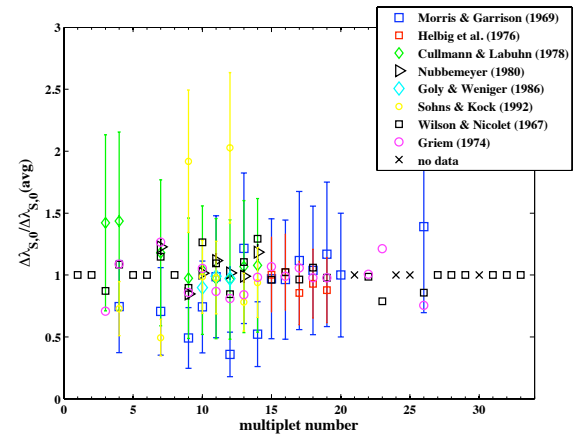

Figure 3: Comparison of various experimental and theoretical Stark broadening coefficients, normalized by the average, for the 33 nitrogen lines listed in Table 1.

American Institute of Aeronautics and Astronautics

The theoretical[9,17] and experimental[18–22] data collected to determine these oscillator strength uncertainties are presented in Figures 1 and 2 for nitrogen multiplets 1–14 and 15–33, respectively. As discussed by Johnston et al.,[6] the present uncertainties were chosen based on the deviation of the post-1970 data (therefore neglecting the Wiese et al. (1966) data[23] and Wilson and Nicolet (1967) data[16]) shown in Figures 4 and 5 from the Wiese et al. (1996) values.[14] However, for the multiplets with only the Wilson and Nicolet (1967)[16] and Wiese et al. (1996) values[14] available (multiplets 1, 2, 4 and 5), the difference between these two values were used in the uncertainty determination. The presently chosen uncertainties are generally higher than those proposed by Wiese et al. (1996), although a few remain the same. A minimum uncertainty of $\pm 10\%$ was chosen because no experimental measurement contained an uncertainty lower than this value. The uncertainties listed in Table 2 for oxygen lines are taken directly from Wiese et al. (1996).

The experimental[24–29] and theoretical data collected to determine the $\Delta\lambda_{S,0}$ uncertainties are shown in Figure 3 for the multiplets listed in Table 1. For the multiplets with only the Wilson and Nicolet values available, an uncertainty of $\pm 75\%$ was assigned based on the comparison with other multiplets, while for the cases with "no data", an uncertainty of $\pm 100\%$ was conservatively chosen. For the multiplets with various measurements available it is noted that, except for multiplets 7, 9, 12, and 14, the measurement uncertainties overlap the averaged value (meaning they overlap the value of 1 in the figure) as well as the nominal values from the other measurements and predictions. Considering this, the uncertainty was chosen to capture the nominal values, relative to the average, from all the measurements and theoretical results.

B.   Atomic Photoionization Cross Sections

Recent theoretical predictions by various researchers of nitrogen[30–32] and oxygen[33,34] photoionization cross sections (σ_{bf}) agree within 10% of each other. However, the comparison of predictions with actual measurements[35–39] is much worse, with the agreement ranging from 30-50%. A complication in the analyses of the measurements is the possible influence of the negative nitrogen ion, which provides an increase in the continuum radiation. The uncertain magnitude of the negative nitrogen ion cross section, which will be discussed later, makes it difficult to subtract out of the continuum measurement to obtain the photoionization contribution. As a tradeoff between the consistency of the theoretical predictions and the poor agreement with the measurements, which depends on how the negative ion is treated, an uncertainty of $\pm 20\%$ is chosen for all the photoionization cross sections of nitrogen and oxygen.

C.   Negative Ion Continuum Cross Sections

As a result of the few theoretical predictions available[40–42] and the difficulty mentioned previously in obtaining cross sections from experimental data[43] (due to the overlapping photoionization contribution), there is significant uncertainty in the negative ion continuum cross section (σ^-).[44] From the wide spread of proposed cross sections, an uncertainty of $\pm 100\%$ is chosen for the negative nitrogen ion. The nominal σ^- values applied in HARA are presented by Johnston et al.[6] The lower limit of the $\pm 100\%$ uncertainty represents neglecting the negative ion contribution entirely.

D.   Molecular Band Oscillator Strengths

The most significant emitting molecular band system in air at the present conditions is the N_2^+ first-negative system. The oscillator strength uncertainty for this band system is chosen as $\pm 10\%$, following comparisons by Langhoff and Bauschilcher.[45] Following Laux and Kruger,[46] the uncertainties for the N_2 first-positive, N_2 second positive, and all NO band systems are chosen as $\pm 10\%$. For the N_2 VUV bands systems[6] (Birge-Hopfield, Worley, Worley-Jenkins, and Carroll-Yoshino), an uncertainty of $\pm 50\%$ is chosen based on the comparisons presented by Stark et al.,[47] Chan et al.,[48] Appleton and Steinberg,[49] and Carter.[50]

E.   Electron-Impact Excitation Rates

For the lunar return conditions of present interest, the electron-impact excitation rates (K_{el}) are the dominant contributors to the non-Boltzmann calculation for both atoms and molecules. The electron-impact excitation rates applied in HARA were presented by Johnston et al.,[7] who also showed that significant uncertainty exists in the chosen values. For example, Figure 4 compares the rates proposed by various researchers[51–54] for an atomic nitrogen transition. The range of values shown in this figure indicate that a one order-of-magnitude uncertainty is appropriate. Other comparisons presented by Johnston[2] for atomic nitrogen and oxygen show

American Institute of Aeronautics and Astronautics

that a one order of magnitude uncertainty is appropriate for all atomic electronic-impact excitation rates. This value is applied in the present study.
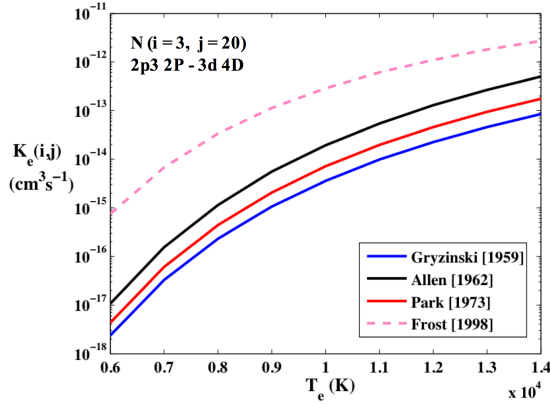

Figure 4: Comparison of electron-impact excitation rates proposed by various researchers for an atomic nitrogen transition.
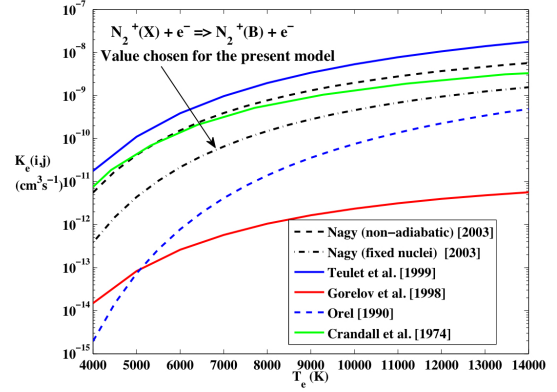

Figure 5: Comparison of electron-impact excitation rates proposed by various researchers for an N_2^+ transition.

A comparison of proposed values[55–57] for the N_2^+ X - B transition, which is the dominant transition for populating the upper state of the strongly emitting N_2^+ first-negative band system, is shown in Figure 5. Ignoring the result of Gorelov et al.,[55] a plus or minus one order of magnitude uncertainty is seen to bound the various values. Johnston[2] shows similar comparisons for other N_2 and N_2^+ rates. Therefore, a one order of magnitude uncertainty is applied in the present study to all molecular electronic impact excitation rates.

V.   Uncertainty Analysis Techniques

Kleb et al.[58] introduced a new method of specifying input uncertainties that could readily be used with a wide range of numerical simulation codes and to create a persistent, in situ means to document model parameter uncertainties. For example, if an input file included an entry such as `parameter = 5.0`, it could be marked up with a tolerance like `parameter = 5.0+/-10%` to a produce "fuzzy" version of the original input file that documented the uncertainty of the input parameters.

In our previous work,[58] we treated all the tolerances in these "fuzzy" files as variabilities (uncertainties with probability distributions) and used the Monte Carlo method to determine the variability in the output. The output variability we found, however, was unexpectedly small and after further investigation,[60, 61] discovered that we were failing victim to a common mistake in the field of risk analysis: treating epistemic uncertainty (uncertainty due to lack of knowledge) as aleatory uncertainty (uncertainty due to chance).

In saying that we knew even uniform distributions for the input parameters was claiming too much. When using any sort of scaled distribution (e.g., normal, triangular, or uniform) for the input parameters, the second fundamental theorem of probability, the Central Limit Theorem,[59] holds sway and produces a normal output distribution with a variance according to,

$$\sigma_{\text{out}} = \sigma_{\text{in}}/\sqrt{N} \tag{1}$$

where N is the number of input distributions and σ_{out} and σ_{in} are the standard deviations of the output and input distributions, respectively. No matter which input parameter probability distributions we chose (e.g., normal, uniform, or triangular), we obtained the same, inexplicably small, output uncertainty.

To overcome this under estimation of the output uncertainty, we set out to perform second-order probability analysis[60, 61] where we would admit that *some* of our inputs should be treated as epistemic uncertainties (unknown within an interval) and not as aleatory uncertainties (variable according to some probability distribution). As detailed in the preceding section, however, *none* of the input parameters we are considering have enough data to justify assigning a probability distribution, and so all input parameters became intervals, devoid of probability distributions.

A result of not having probability distributions for the parameter uncertainties is that the nominal parameter values and the resulting nominal (or mean) value of the function (in this case the radiative flux) are no long defined. In other words, the nominal parameters are arbitrary. Hence, they do not represent the

American Institute of Aeronautics and Astronautics

most probable value, as they would if, for example, a Gaussian distribution was assumed. The consequence of an arbitrary nominal is indicated in Figure 6, which shows the variability around various sets of nominal values obtained by assuming uniform probability distributions for the epistemic input parameters. The thick curve to represents the radiative flux predicted by HARA when using the nominal parameters chosen in the development of the code when some input parameters are specified to have aleatory uncertainties (variability due to chance). The other curves represent the variability if different nominal parameters were chosen within the specified uncertainty intervals. These curves are just as relevant as the initial nominal because the probability distributions of the inputs are uniform. This is known as a second-order probability analysis, i.e., treating aleatory and epistemic uncertainties separately. It is clear from this figure that the variation of the nominal (or mean) is greater than the 2-σ variability of any single case. The epistemic uncertainty approaches applied in this work compute this variation in the mean, but

Figure 6: **Example of second-order probability analysis that contains both aleatory and epistemic uncertainties.**

for our case, we have no underlying distributions due to aleatory input uncertainties but single deterministic output values due to only having epistemic uncertainties.
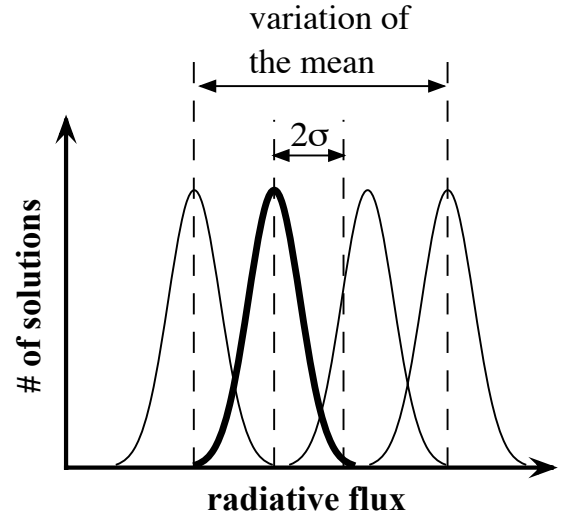
As shown by Kreinovich et al.,[62] only two methods can accommodate epistemic uncertainty. The first is direct numerical differentiation and the second is the Monte Carlo-based, Cauchy Deviates Method.[63] Given sufficiently small differences for the former and a sufficiently large number of samples for the later, both techniques will give the same maximum possible output uncertainty due to input parameter uncertainty intervals. For the present study, the numerical differentiation method required exactly 3627 HARA evaluations (which is equal to the number of uncertainty parameters considered) while the Cauchy Deviates method required less than 500 HARA evaluations. The relatively small computational time required by the HARA code ($\tilde{3}0$ seconds for a shock layer line of sight) made both approaches feasible. Therefore, they were both applied to assure proper implementation. The resulting uncertainties were found to agree within 5%. The following subsections outline each method.

A. Numerical Differentiation

Direct numerical differentiation is used to obtain sensitivity derivatives of outputs with respect to inputs. Consider an output function, y, that is a function of a set of n input parameters, $x_1, \ldots, x_n$,

$$y = f(x_1, \ldots, x_n). \tag{2}$$

By applying the chain rule and linearizing, we can determine the maximum possible uncertainty in y given the uncertainty in inputs,

$$\Delta y = |s_1| \cdot \Delta x_1 + \ldots + |s_n| \cdot \Delta x_n \tag{3}$$

where s_i is the linearized sensitivity derivative of f with respect to x_i,

$$s_i = \frac{\Delta f}{\Delta x_i}. \tag{4}$$

Here Δx_i is typically taken as the width of the uncertainty interval provided that the function remains linear over that range.

B. Cauchy Deviates Method

The Cauchy Deviates Method[63] is a Monte Carlo technique for computing uncertainty when inputs have epistemic uncertainty, i.e., only input intervals are known due to lack of knowledge.

American Institute of Aeronautics and Astronautics

The basic steps of any Monte Carlo method are as follows:

1. Define scope of the problem. For the present study this involves the simulation, using the HARA code, of the radiative flux emitted from a high temperature gas.

2. Assign uncertainties to model input parameters. The previous section lists the uncertainties presently considered for the HARA code.

3. Randomly sample inputs, run, and repeat until the statistics have converged.

4. Compute input-output correlations, scatter plots, sensitivities, and other quantities of interest.

Each "fuzzy" file is randomly sampled to provide a given realization, the underlying code is run, and these steps are repeated until statistical convergence of the outputs is reached. The overall work flow is depicted in Figure 7.

Specifically, the Cauchy Deviates Method[63] has the following steps:

1. Compute the nominal case, i.e., $y = f(x_1, \ldots, x_n)$.

2. For $k = 1, 2, \ldots, N$, where N is the number of samples, repeat the following:

   (a) Compute Cauchy distributed values, $c_i^{(k)} = \tan(\pi \cdot (r_i^{(k)} - 0.5))$ where $r_i^{(k)}$ is a random number uniformly distributed between 0 and 1;

   (b) Store the maximum of the absolute values, $c_{max}^{(k)} = \max|c_i^{(k)}|$;

   (c) Compute sampled input, $x_i^{(k)} = x_i + \Delta_i \cdot c_i^{(k)}/c_{max}^{(k)}$;

   (d) Compute the scaled difference, $d^{(k)} = c_{max}^{(k)}(f(x^{(k)}) - y)$;

3. Solve $\frac{\Delta^2}{\Delta^2+(d^{(1)})^2} + \cdots + \frac{\Delta^2}{\Delta^2+(d^{(N)})^2} = N/2$ by method of bisection on the interval $[0, d_{max}^{(k)}]$.

A useful property of Cauchy Deviates Method is that it has an estimated confidence interval proportional to the number of samples and independent of the number of input parameters. So while the work associated with direct numerical differentiation scales linearly with number of input parameters under consideration, the Cauchy Deviates Method scales only with the desired level of confidence in the output uncertainty.
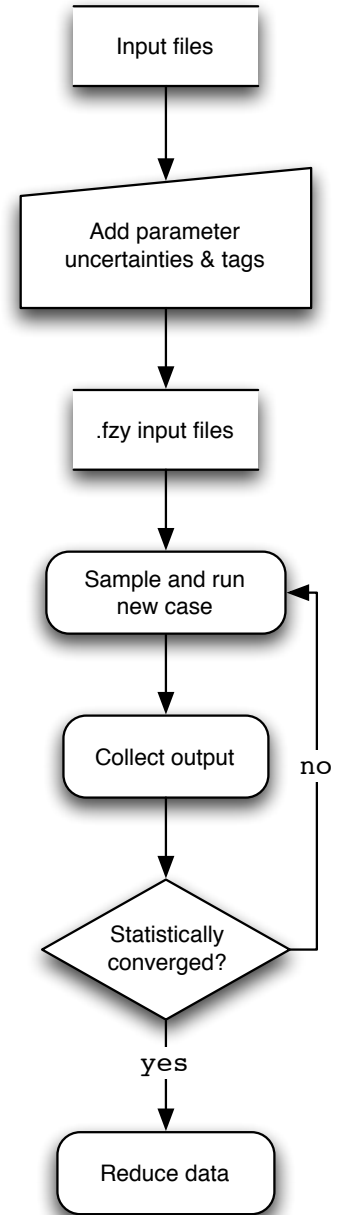

Figure 7: Simulation architecture.

VI. Results

A. Dual-Layer Slab Case

The radiative flux along the stagnation line of a peak heating lunar return shock layer may be represented approximately with two constant property layers of air in chemical equilibrium. This simplified problem avoids the complexity of a variable-property shock layer while maintaining the fundamental characteristics (significant to radiation) of peak heating lunar return shock layer. The case studied here is shown in Figure 8. The first layer (Layer 1), which has a thickness of 15 cm and a temperature of 10,000 K, represents the inviscid region of the shock-layer, while the boundary layer is represented by the 1 cm layer at 5,000 K (Layer 2). A pressure of 0.5 atm
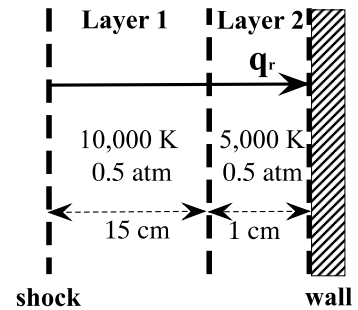

Figure 8: Dual-layer slab configuration.

American Institute of Aeronautics and Astronautics

is assigned to both layers. The radiative flux resulting from both layers and directed towards the wall, as shown in Figure 8, is defined as q_r and will be the subject of the present study.

The radiative flux spectrum and resulting cumulative flux are shown in Figure 9 for Layers 1 and 2. As expected, the absorption from Layer 2 is located entirely above 6 eV (VUV) and reduces the total flux from 380 to 323 W/cm^2. The absorption seen between 12 and 14 eV is due mostly to the N_2 Birge-Hopfield band systems, while that between 14 and 16 eV is from the N and O bound-free continuum. The emission contributions of each radiative mechanism is indicated in Figure 10, which shows the radiative flux from Layer 1 assuming emission from only the specified mechanism, but absorption from all mechanisms. The strong contribution from atomic nitrogen atomic lines is noted followed by the atomic nitrogen bound-free continuum.
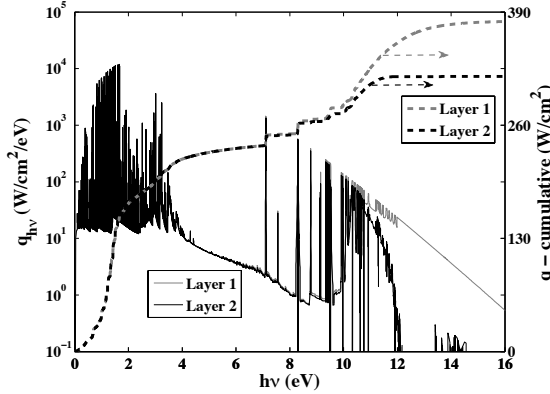

Figure 9: Spectrum and cumulative flux at the edge of Layers 1 and 2.
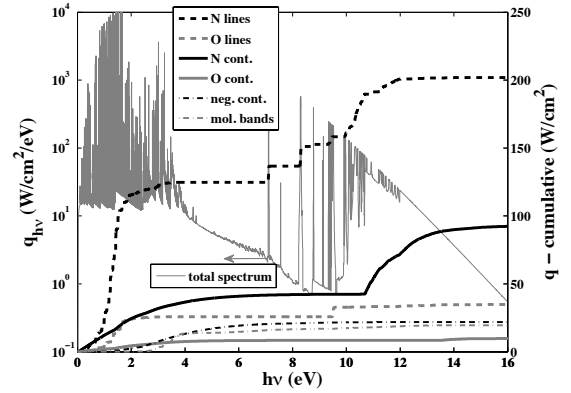

Figure 10: Spectrum and radiative flux components from Layer 1.

Applying to this case the previously described uncertainty approach along with the previously chosen parameter uncertainty intervals, radiative flux uncertainty values of ±93.1 W/cm^2 (25%) and ±93.9 W/cm^2 (29%) were calculated for Layers 1 and 2, respectively. For both cases, the uncertainty below 6 eV (non-VUV) was found to be ±66.4 W/cm^2 (28%). Meanwhile, treating the input uncertainties as aleatory (known variability due to stochastic process) yields only ±7%.

The contributions of the various parameter groups to these uncertainties are listed in Tables 3 and 4 in order of largest to smallest contribution. For both layers the top three parameters are the atomic nitrogen oscillator strengths (f_{ij} (N)), atomic nitrogen Stark broadening widths ($\Delta\lambda_{S,0}$ (N)), negative ion cross-section (σ^-), and atomic nitrogen bound-free cross-sections (σ_{bf} (N)). The molecular band oscillator strength contribution is larger for Layer 2 because the Birge-Hopfield band system contributes significantly to the vacuum ultraviolet absorption present in Layer 2. This is indicated in Table 5, which lists the uncertainty contribution from the top 15 individual parameters for Layer 2. Note that $\Delta\lambda_{S,0}$ values for both VUV and non-VUV nitrogen lines are present in this list. Also note that while there are fewer f_{ij} than $\Delta\lambda_{S,0}$ values in this list of the top 15 contributors, the contribution from all f_{ij} values is greater, as shown in Table 4. This is a result of the f_{ij} values influencing the radiative flux from the numerous weak atomic lines, which contribute when added together, while the radiative flux from these lines is essentially independent of $\Delta\lambda_{S,0}$. Furthermore, the 35 strong nitrogen lines listed in Table 1 result in roughly half of the total nitrogen $f_{ij}(N)$ uncertainty contribution, while they result in nearly 80% of the total $\Delta\lambda_{S,0}(N)$ contribution. The f_{ij}-OP (N) refers to the group of all OP nitrogen lines (so it does not actually refer to an individual parameter).

American Institute of Aeronautics and Astronautics

Table 3: Total uncertainty contribution from parameter groups for Layer 1.

Rank	Parameter	$\pm q_r$ (W/cm^2)	$\pm q_r$ (%)
1	f_{ij} (N)	31.1	8.2
2	$\Delta\lambda_{S,0}$ (N)	22.3	5.9
3	σ^-	20.0	5.3
4	σ_{bf} (N)	9.2	2.4
5	$\Delta\lambda_{S,0}$ (O)	4.2	1.1
6	f_{ij} (O)	3.1	0.9
7	f_{ij} (Bands)	2.0	0.5
8	σ_{bf} (O)	1.3	0.3
	Total	93.1	24.5

Table 4: Total uncertainty contribution from parameter groups for Layer 2.

Rank	Parameter	$\pm q_r$ (W/cm^2)	$\pm q_r$ (%)
1	f_{ij} (N)	29.7	9.2
2	$\Delta\lambda_{S,0}$ (N)	20.7	6.4
3	σ^-	20.0	6.2
4	σ_{bf} (N)	7.9	2.4
5	f_{ij} (Bands)	7.4	2.3
6	$\Delta\lambda_{S,0}$ (O)	4.0	1.2
7	f_{ij} (O)	3.0	0.9
8	σ_{bf} (O)	1.4	0.4
	Total	93.9	29.0

Table 5: Top 15 uncertainty contributions from individual parameters for Layer 2.

Rank	Parameter	Uncertainty ($\pm\%$)	$\pm q_r$ (W/cm^2)	$\pm q_r$ (%)
1	σ^- (N^-)	100	20.0	6.2
2	f_{ij} (N_2 Birge-Hopfield)	50	4.8	1.5
3	$\Delta\lambda_{S,0}$ (N) — 174.36 nm	50	2.6	0.8
4	σ_{bf} (N 2p3 2P / level 3)	10	1.8	0.6
5	$\Delta\lambda_{S,0}$ (N) — 1011.7 nm	50	1.5	0.5
6	$\Delta\lambda_{S,0}$ (N) — 1052.6 nm	75	1.4	0.4
7	f_{ij}-OP (N)	30	1.4	0.4
8	$\Delta\lambda_{S,0}$ (N) — 149.3 nm	30	1.3	0.4
9	$\Delta\lambda_{S,0}$ (N) — 869.4 nm	30	1.3	0.4
10	$\Delta\lambda_{S,0}$ (N) — 821.4 nm	30	1.2	0.3
11	f_{ij} (N) — 919.8 nm	50	1.2	0.3
12	f_{ij} (N_2^+ first-negative)	10	1.2	0.3
13	f_{ij} (N) — 120.0 nm	20	1.1	0.3
14	f_{ij} (N) — 174.36 nm	20	1.1	0.3
15	$\Delta\lambda_{S,0}$ (O) — 821.4 nm	50	1.1	0.3

B. Lunar Return Shock Layer

The stagnation-line radiative flux for a 3.6 m sphere at 10.2 km/s and 60 km is studied in this section. This configuration approximates the Orion stagnation region at peak heating lunar return conditions. A two-temperature thermochemical nonequilibrium LAURA[64, 65] flowfield was applied, which contains radiation-flowfield coupling with the nominal radiative flux. The stagnation line temperature and nominal radiative flux profiles are shown in Figure 11, with radiative flux at wall equal to 206 W/cm^2.

The calculated uncertainty contributions from the grouped parameters are shown in Table 6 for the lunar return case. The total uncertainty for this case is ± 61.9 W/cm^2 ($\pm 30\%$) as compared to $\pm 5\%$ when treating the input uncertainties as aleatory (known but variable according to chance).

Except for the presence of the electron-impact excitation rates (K_{el}) values for this case (they did not contribute to the simplified case because it was in chemical equilibrium), the results in Table 6 are very similar

Figure 11: Stagnation-line temperature and radiative flux profiles for lunar return.

to the dual-layer slab results presented previously in Table 4. Further similarity is apparent from Table 7, which presents the top 10 individual parameter uncertainty contributions. The K_{el} (N_2^+ (X - B)) value listed in this table represents the electron-impact excitation rate for the upper state of the strongly emitting N_2^+ first-negative band system. Figure 12 shows the uncertainty bars at each point through the shock layer for the wall-directed radiative flux. The uncertainty is seen to consist of a gradual build-up, starting at shock ($z = 18$ cm) and increasing as the wall is approached at $z = 0$.
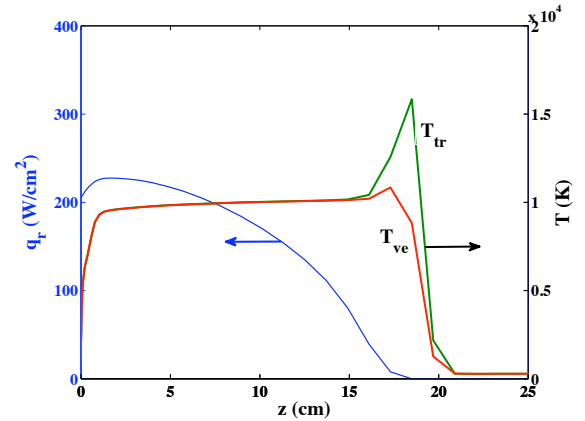
Table 6: Total uncertainty contribution from parameter groups for the lunar return case.

Rank	Parameter	$\pm q_r$ (W/cm^2)	$\pm q_r$ (%)
1	f_{ij} (N)	18.4	8.9
2	$\Delta\lambda_{S,0}$ (N)	12.9	6.3
3	σ^-	8.6	4.2
4	σ_{bf} (N)	5.7	2.8
5	K_{el} (Bands)	4.4	2.1
6	f_{ij} (Bands)	3.9	1.9
7	K_{el} (N)	2.4	1.2
8	$\Delta\lambda_{S,0}$ (O)	2.6	1.3
9	f_{ij} (O)	1.8	0.9
10	σ_{bf} (O)	0.76	0.4
11	K_{el} (O)	0.44	0.2
	Total	61.9	30.0

Table 7: Top 10 uncertainty contributions from individual parameters for lunar return case.

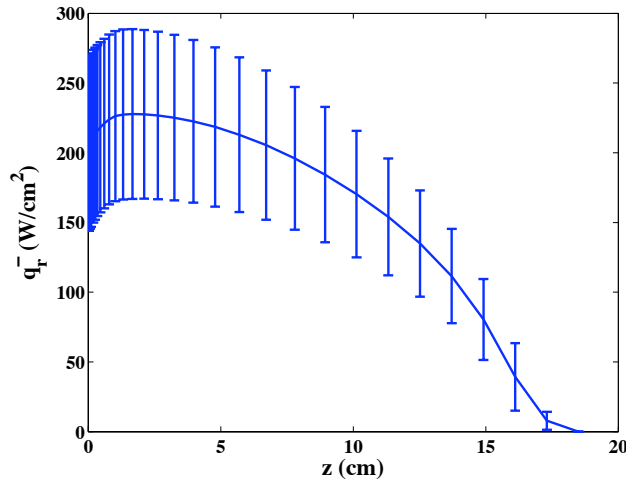| Rank	Parameter	Uncertainty	$\pm q_r$ (W/cm^2)	$\pm q_r$ (%)
1	σ^- (N^-)	100%	8.6	4.2
2	σ_{bf} (N 2p3 2P / level 3)	10%	2.3	1.1
3	f_{ij} (N_2 Birge-Hopfield)	50%	1.9	0.9
4	$\Delta\lambda_{S,0}$ (N) — 174.36 nm	50%	1.6	0.8
5	K_{el} (N_2^+ (X - B))	$O(1)$ mag.	1.6	0.8
6	$\Delta\lambda_{S,0}$ (N) — 1011.7 nm	50%	1.1	0.5
7	$\Delta\lambda_{S,0}$ (N) — 149.3 nm	30%	0.9	0.4
8	$\Delta\lambda_{S,0}$ (N) — 869.4 nm	30%	0.8	0.4
9	f_{ij}-OP (N)	30%	0.8	0.4
10	$\Delta\lambda_{S,0}$ (N) — 1052.6 nm	75%	0.8	0.4

Figure 12: Stagnation-line radiative flux profile with uncertainty bars for the lunar return case.

C. Fire II: 1636 and 1643 Second Trajectory Points

The radiative heating for the Fire II flight experiment[66] has been studied previously with HARA coupled to viscous shock-layer (VLS) flowfield.[3] For the present study, the LAURA flowfield solver is applied instead, as it was for the lunar-return case considered in the previous section. Two trajectory points are considered presently. The 1636 second case ($U_{inf} = 11.31$ km/s, altitude = 71.02 km) was chosen because it contains significant regions of thermochemical nonequilibrium while also producing significant radiative heating. The 1643 second case ($U_{inf} = 10.48$ km/s, altitude = 53.04 km) was chosen because it represents the trajectory point of peak radiative heating.

For the Fire 1636 case, the grouped and individual parameter uncertainty contributions are listed in Tables 8 and 9, respectively. The total uncertainty for this case is ±26.4%, with the nominal radiative flux[a] equal to 71.9 W/cm^2, which again is much higher than ±4.6% if one claims to know input parameter distributions, means, and variability.

For the Fire 1643 case, the grouped and individual parameter uncertainty contributions are listed in Tables 10 and 11, respectively. The total uncertainty for this case is ±28.9%, with the nominal radiative flux equal to 492.9 W/cm^2, where uncertainty based on variability gives ±5.1%.

---

[a]This nominal radiative flux shown here is slightly different than that presented by Johnston et al.[3] because the shock capturing of the LAURA flowfield produces a slightly different nonequilibrium region than the discrete shock VSL approach applied previously.

American Institute of Aeronautics and Astronautics

Table 8: Total uncertainty contribution from parameter groups for the Fire 1636 case.

Rank	Parameter	$\pm q_r$ (W/cm^2)	$\pm q_r$ (%)
1	f_{ij} (N)	6.7	9.3
2	$\Delta\lambda_{S,0}$ (N)	5.0	7.0
3	K_{el} (Bands)	2.9	4.0
4	σ_{bf} (N)	2.8	3.9
5	f_{ij} (Bands)	2.4	3.4
6	K_{el} (N)	2.3	3.2
7	$\Delta\lambda_{S,0}$ (O)	0.7	0.9
8	σ^-	0.5	0.7
9	f_{ij} (O)	0.4	0.6
10	K_{el} (O)	0.4	0.6
11	σ_{bf} (O)	0.2	0.3
	Total	24.3	26.4

Table 9: Top 10 uncertainty contributions from individual parameters for the Fire 1636 case.

Rank	Parameter	Uncertainty	$\pm q_r$ (W/cm^2)	$\pm q_r$ (%)
1	K_{el} (N_2^+ (X - B))	$O(1)$ mag.	2.1	2.8
2	σ_{bf} (N 2p3 2P / level 3)	10%	1.2	1.6
3	σ_{bf} (N 2p3 2D / level 2)	10%	1.1	1.5
4	f_{ij} (N_2 Birge-Hopfield)	50%	0.8	1.1
5	f_{ij} (N_2 Worley)	50%	0.6	0.9
6	$\Delta\lambda_{S,0}$ (N) — 174.36 nm	50%	0.6	0.9
7	$\Delta\lambda_{S,0}$ (N) — 149.3 nm	30%	0.5	0.7
8	σ^- (N^-)	100%	0.5	0.7
9	f_{ij} (N_2^+ first-negative)	50%	0.4	0.5
10	K_{el} (N_2^+ (A - B))	$O(1)$ mag.	0.4	0.5

Table 10: Total uncertainty contribution from parameter groups for the Fire 1643 case.

Rank	Parameter	$\pm q_r$ (W/cm^2)	$\pm q_r$ (%)
1	f_{ij} (N)	44.9	9.1
2	$\Delta\lambda_{S,0}$ (N)	33.5	6.8
3	σ^-	18.8	3.8
4	σ_{bf} (N)	13.5	2.7
5	f_{ij} (Bands)	11.1	2.2
6	$\Delta\lambda_{S,0}$ (O)	5.9	1.2
7	K_{el} (Bands)	5.5	1.1
8	f_{ij} (O)	3.6	0.7
9	K_{el} (N)	3.0	0.6
10	σ_{bf} (O)	1.8	0.4
11	K_{el} (O)	0.7	0.1
	Total	142.4	28.9

Table 11: Top 10 uncertainty contributions from individual parameters for the Fire 1643 case.

Rank	Parameter	Uncertainty (%)	$\pm q_r$ (W/cm^2)	$\pm q_r$ (%)
1	σ^- (N^-)	100	1.8	3.8
2	σ_{bf} (N 2p3 2P / level 3)	10	5.7	1.2
3	f_{ij} (N_2 Birge-Hopfield)	50	5.3	1.1
4	$\Delta\lambda_{S,0}$ (N) — 174.36 nm	50	5.0	1.0
5	$\Delta\lambda_{S,0}$ (N) — 149.3 nm	30	2.6	0.5
6	f_{ij} (N_2 Worley)	50	2.2	0.4
7	f_{ij} (N) — 174.36 nm	20	2.0	0.4
8	$\Delta\lambda_{S,0}$ (O) — 130.35 nm	50	2.0	0.4
9	$\Delta\lambda_{S,0}$ (N) — 869.4 nm	30	2.0	0.4
10	$\Delta\lambda_{S,0}$ (N) — 821.4 nm	30	1.7	0.3

Comparing the 1636 results (Tables 8 and 9) with the 1643 results (Tables 10 and 11) provides insight into the differences in the radiation uncertainty between a relatively strong nonequilibrium (1636) and equilibrium (1643) cases. As expected, the electron impact excitation rates (K_{el} (Bands), K_{el} (N), and K_{el} (O)), which govern the non-Boltzmann state populations and therefore the nonequilibrium radiation, are seen to contribute $\pm7.8\%$ for 1636 and only $\pm1.8\%$ for 1643. Furthermore, the individual electron impact excitation rates, K_{el} (N_2^+ (X - B)) and K_{el} (N_2^+ (A - B)), which govern the upper state of the N_2^+ first-negative band system, are among the top 10 contributors for 1636, while no electron impact excitation rates rank in the top 10 for 1643.

The negative ion (σ^-) contribution is smaller for the 1636 case because the shock layer temperatures are higher than the 1643 case, which decreases the negative ion number density. However, the negative ion contribution is smaller for the 1643 case than the lunar return case studied in the previous section. This is a result of the Fire shock layer being significantly thinner (4 cm) than the lunar return case (20 cm), which means the radiation is less optically thick and the continuum radiation contributes less relative to the atomic lines.

An interesting result of the present analysis is the uncertainty of the intensity between 0 and 6 eV (I (0–6 eV)), or above 200 nm. This quantity was measured by the Fire II radiometer,[66] and is therefore of particular interest. The present analysis results in I (0–6 eV) of 4.8 ± 1.5 W/cm^2/sr for the 1636 case, which compares well with the measured result of 4.9 ± 1.1 W/cm^2/sr. For the 1643 case, the present analysis results in I (0–6 eV) in 51.1 ± 13.8 W/cm^2/sr, which overlaps the error bounds of the measured result of 63.0 ± 14.5 W/cm^2/sr.

American Institute of Aeronautics and Astronautics

VII.   Concluding Remarks

By using a new uncertainty markup technique, direct numerical differentiation and the Cauchy Deviates Method were used to investigate the uncertainty of lunar return shock layer flowfield radiation due to epistemic uncertainty in the radiation modeling parameters. It is shown that previous uncertainty analyses based on aleatory uncertainty led to unjustifiably small uncertainty levels.

The High-temperature Aerothermodynamic Radiation Algorithm (HARA) was applied in this study for the radiation predictions, and the following parameter uncertainties were considered: atomic line oscillator strengths, atomic line Stark broadening widths, atomic photoionization cross sections, negative ion photodetachment cross sections, molecular bands oscillator strengths, and electron impact excitation rates. An assessment of the uncertainties for each of these parameters was conducted based on available published data.

A simplified shock layer problem was considered to isolate the uncertainty contributions from the strongly emitting and strongly absorbing regions of the shock layer. This simplified problem consisted of two constant property layers of equilibrium air with the thickness, pressure, and temperature of each layer chosen to represent the inviscid region and boundary layer of a typical Lunar return shock layer. The results of this simplified problem show that for conditions of chemical equilibrium, the atomic nitrogen oscillator strengths and Stark broadening widths in both the vacuum ultraviolet and infrared spectral regions are the dominant uncertainty contributors, along with the negative ion continuum.

Following this simplified case, three stagnation line shock layer cases were studied: a typical Lunar return case consisting of a 3.6 m sphere at 10.2 km/s and 60 km, and the Fire II 1636 and 1643 second trajectory point cases. These cases considered actual variable property stagnation line flowfields obtained from the LAURA flowfield solver. For the strongly equilibrium Lunar return and Fire 1643 cases, the resulting uncertainties were very similar to the simplified case. Conversely, the relatively nonequilibrium 1636 case was subject to a significantly larger influence from electron impact excitation rates of both atoms and molecules. For all cases, the total uncertainty was found to be around $\pm 30\%$.

An interesting result of the present analysis is that no individual parameter contributed more than 7% to the total uncertainty. Also, although the atomic nitrogen oscillator strengths contributed the most uncertainty as a group for each case, they represented only one of the top 10 contributing individual parameters. This is a result of the many small oscillator strength uncertainties combining to a significant value. The Stark broadening widths contributed as many as 5 of the top 10 individual parameters, but their group contribution was smaller because they have no influence on the numerous weak optically thin lines.

Acknowledgments

About the Authors

BIL KLEB, a lifetime AIAA member, has worked in the area of computational aerothermodynamics at NASA's Langley Research Center for the past 18 years. During this time, he pioneered the first full-vehicle reentry simulation of the Shuttle Orbiter and earned an MBA from The College of William and Mary and a PhD of Aerospace Engineering from the University of Michigan.

Since 1999, Bil has also been a part of the Agile software development community,[b] and for the past six years, a steward of the FUN3D software development team.[c]

Email: Bil.Kleb@NASA.gov

CHRISTOPHER JOHNSTON, an AIAA member with a Ph.D. in Aerospace Engineering from Virginia Tech, has been a member of NASA Langley Research Center's Aerothermodynamics Branch since 2006.

Email: Christopher.O.Johnston@NASA.gov

---

[b]agilemanifesto.org, last accessed January 10th, 2008.
[c]fun3d.larc.nasa.gov, last accessed January 10th, 2008.

Colophon

This document was typeset by LATEX in Computer Modern font with the AIAA package,[d] version 3.8. Also employed were the `array`, `booktabs`, `color`, `dcolumn`, `fancyvrb`, `hyperref`, `subfig`, `svninfo`, `threeparttable`, `varioref`, and `wrapfig` packages.

References

[1] Bose, D., McCorkle, E., Thompson, C., Bogdanoff, D., Prabhu, D. K., Allen, G. A., and Grinstead, J., "Analysis and Model Validation of Shock Layer Radiation in Air," AIAA Paper 2008–1246, Jan. 2008.

[2] Johnston, C. O., *Nonequilibrium Shock-Layer Radiative Heating for Earth and Titan Entry*, Ph.D. thesis, Virginia Polytechnic Institute and State University, 2006.

[3] Johnston, C. O., Hollis, B., and Sutton, K., "Nonequilibrium Stagnation-Line Radiative Heating for Fire II," *Journal of Spacecraft & Rockets*, Nov.-Dec. 2008.

[4] Grinstead, J., Wilder, M., Olejniczak, J., Bogdanoff, D., Allen, G., and Danf, K., "Shock-Heated Air Radiation Measurements at Lunar Return Conditions," AIAA Paper 2008–1244, Jan. 2008.

[5] Johnston, C. O., "A Comparison of EAST Shock Tube Radiation Measurements with a New Air Radiation Model," AIAA Paper 2008–1245, Jan. 2008.

[6] Johnston, C. O., Hollis, B. R., and Sutton, K., "Spectrum Modeling for Air Shock-Layer Radiation at Lunar-Return Conditions," *Journal of Spacecraft & Rockets*, Sep.-Oct. 2008.

[7] Johnston, C. O., Hollis, B., and Sutton, K., "Non-Boltzmann Modeling for Air Shock Layers at Lunar Return Conditions," *Journal of Spacecraft & Rockets*, Sep.-Oct. 2008.

[8] Ralchenko, Y., "NIST Atomic Spectra Database, Version 3.1.0," physics.nist.gov/PhysRefData/ASD/, July 2006, last accessed September 3rd, 2007.

[9] The Opacity Project Team, *The Opacity Project*, Vol. 1, Bristol and Philadelphia: Institute of Physics Publishing, 1995.

[10] Cunto, W., Mendoza, C., Ochsenbein, F., and Zeippen, C., "TOPbase at the CDS," *Astronomy and Astrophysics*, Vol. 275, Aug. 1993, pp. L5–L8, see also vizier.u-strasbg.fr/topbase/topbase.html.

[11] Chambers, L. H., "Predicting Radiative Heat Transfer in Thermochemical Nonequilibrium Flow Fields," NASA TM 4564, 1994.

[12] Johnston, C. O., Hollis, B. R., and Sutton, K., "Radiative Heating Methodology for the Huygens Probe," *Journal of Spacecraft & Rockets*, Vol. 44, No. 5, 2007, pp. 993–1002.

[13] Park, C., "Stagnation-Point Radiation for Apollo 4," *AIAA Journal of Thermophysics and Heat Transfer*, Vol. 18, 2004, pp. 349–357.

[14] Wiese, W. L., Fuhr, J. R., and Deters, T. M., "Atomic Transition Probabilities of Carbon, Nitrogen, and Oxygen," *Journal of Physical and Chemical Reference Data Monograph*, , No. 7, 1996.

[15] Griem, H. R., *Spectral Line Broadening by Plasmas*, Academic Press, New York, 1974.

[16] Wilson, K. H. and Nicolet, W. E., "Spectral Absorption Coefficients of Carbon, Nitrogen, and Oxygen Atoms," *Journal of Quantitative Spectroscopy and Radiative Transfer*, Vol. 7, 1967, pp. 891–941.

[17] Hibbert, A., Biemont, E., Godefroid, M., and Vaeck, N., "New Accurate Transition Probabilities for Astrophysically Important Lines of Neutral Nitrogen," *Astronomy and Astrophysics Supplement Series*, Vol. 88, 1991, pp. 505–524.

[18] Goldbach, C., Martin, M., Nollez, G., Plomdeur, P., Zimmerman, J.-P., and Babic, D., "Oscillator Strength Measurements in the Vacuum Ultraviolet: I The Strong 1243, 1493, 1743 Angstrom Multiplets of Neutral Nitrogen," *Astronomy and Astrophysics*, Vol. 161, 1986, pp. 47–54.

[19] Goldbach, C., Ludke, T., Martin, M., and Nollez, G. D., "Oscillator Strength Measurements in the Vacuum Ultraviolet: V. Neutral Nitrogen Lines in the 950–1200 Angstrom Range," *Astronomy and Astrophysics*, Vol. 266, 1992, pp. 605–612.

[20] Goldbach, C. and Nollez, G. D., "Oscillator Strength Measurements in the Vacuum Ultraviolet: III. Weak Lines of Neutral Nitrogen," *Astronomy and Astrophysics*, Vol. 201, 1988, pp. 189–193.

[21] Zhu, Q., Bridges, J. M., Hahn, T., and Wiese, W. L., "Atomic Transition-Probability Measurements for Prominent Spectral Lines of Neutral Nitrogen," *Physical Review A*, Vol. 40, 1989, pp. 3721–3726.

[22] Musielok, J., Wiese, W. L., and Veres, G., "Atomic Transition Probabilities and Tests of the Spectroscopic Coupling Scheme for N I," *Physical Review A*, Vol. 51, 1995, pp. 3588–3597.

[23] Wiese, W. L., Smith, M. W., and Glennon, B. M., "Atomic Transition Probabilities, Vol. 1, Hydrogen through Neon," NSRDS-NBS 4, National Bureau of Standards, May 1966.

[24] Morris, J. C. and Garrison, R. L., "Measurements of the Radiation Emitted f-Values and Stark Half-Widths for the Strong Vacuum Ultraviolet Lines of O I and N I," *Physical Review*, Vol. 188, 1969, pp. 112–118.

[25] Helbig, V., Kelleher, D. E., and Wiese, W. L., "Stark Broadening Study of Neutral Nitrogen Lines," *Physical Review A*, Vol. 14, 1974, pp. 1082–1093.

[26] Cullmann, E. and Labuhn, F., "Stark Broadening of Nitrogen (I) Vacuum-U.V. Lines Using a Wall-Stabalized Arc," *Journal of Quantitative Spectroscopy and Radiative Transfer*, Vol. 20, 1978, pp. 205–209.

[27] Nubbemeyer, H., "Experimental Ion Contributions to the Stark Broadening of Neutral Nitrogen Spectral Lines in the Vacuum UV," *Physical Review A*, Vol. 22, 1980, pp. 1034–1040.

[28] Goly, A. and Weniger, S., "Stark Broadening of Some C(I) and N(I) Vacuum Ultraviolet Lines," *Journal of Quantitative Spectroscopy and Radiative Transfer*, Vol. 36, 1986, pp. 147–161.

---

[d] aiaa-latex.googlecode.com, last accessed January 12th, 2008.

[29]Sohns, E. and Kock, M., "Plasma Diagnostics Based on Self-Reversed Lines-II. Application to Nitrogen, Carbon, and Oxygen Arc Measurements in the Vacuum Ultraviolet," *Journal of Quantitative Spectroscopy and Radiative Transfer*, Vol. 47, 1992, pp. 335–343.

[30]Nahar, S. N. and Pradhan, A. K., "Electron-Ion Recombination Rate Coefficients, Photoionization Cross-Sections, and Ionization Fractions for Astrophysically Abundant Elements. I. Carbon and Nitrogen," *The Astrophysical Journal Supplement Series*, Vol. 111, 1997, pp. 339–355.

[31]Bell, K. L. and Berrington, K. L., "Photoionization of the 4So Ground State of Atomic Nitrogen and Atomic Nitrogen 4So–4P Oscillator Strengths," *Journal of Physics B*, Vol. 24, 1991, pp. 933–941.

[32]Bell, K. L. and Berrington, K. L., "Photoionization of Excited States of Atomic Nitrogen," *Journal of Physics B*, Vol. 25, 1992, pp. 1209–1216.

[33]Nahar, S. N., "Photoionization Cross Sections and Oscillator Strengths for Oxygen Lines: O I – O VII," *Physical Review A*, Vol. 58, 1998, pp. 3766–3782.

[34]Tayal, S. S., "Resonant Photoionization Cross Sections and Branching Ratios for Atomic Oxygen," *Physical Review A*, Vol. 65, 2002, pp. 032724–+.

[35]Morris, J. C., Krey, R. U., and Bach, G. R., "The Continuum Radiation of Oxygen and Nitrogen for Use in Plasma Temperature Determination," *Journal of Quantitative Spectroscopy and Radiative Transfer*, Vol. 6, 1966, pp. 727–740.

[36]Thomas, G. M. and Menard, W. A., "Measurements of the Continuum and Atomic Line Radiation from High Temperature Air," *AIAA Journal*, Vol. 5, No. 12, 1967, pp. 2214–2223.

[37]Marrone, P. V. and Wurster, W. H., "Measurement of Atomic Nitrogen and Carbon Photoionization Cross Sections Using Shock Tube Vacuum Ultraviolet Spectroscopy," *Journal of Quantitative Spectroscopy and Radiative Transfer*, Vol. 11, 1971, pp. 327–348.

[38]Ciffone, D. L. and Borucki, J. G., "Spectral Measurements of Nitrogen Continuum Radiation Behind Incident Shocks at Speeds up to 13 km/sec," *Journal of Quantitative Spectroscopy and Radiative Transfer*, Vol. 11, 1971, pp. 1291–1310.

[39]Cooper, D. M., "Spectral Intensity Measurements from High-Pressure Nitrogen Plasma," *Journal of Quantitative Spectroscopy and Radiative Transfer*, Vol. 12, 1972, pp. 1175–1189.

[40]Moskvin, Y. V., "Cross-Section Photo-Detachment of the Negative Nitrogen Ion," *Optics and Spectroscopy*, Vol. 28, 1970, pp. 356–356.

[41]Asinovskii, E. I., Kirillin, A. V., and Kobzev, G. A., "Continuous Radiation of Nitrogen Plasma," *High Temperature*, Vol. 6, 1968, pp. 710–712.

[42]Soon, W. H. and Kunc, J. A., "Nitrogen-Plasma Continuum Emission Associated with $N^-(^3P)$ and $N^-(^1D)$ ions," *Physical Review A*, Vol. 41, 1990, pp. 4531–4533.

[43]Konkov, A. A., Nikolaev, V. M., and Plastinin, Y. A., "On the Intensity of Emission Continuum of the Negative Nitrogen Atom," *Optics and Spectroscopy*, Vol. 25, 1968, pp. 380–382.

[44]D'Yachkov, L. G., Golubev, O. A., Kobzev, G. A., and Vargin, A. N., "Studies of Continuum Radiation from Nitrogen, Oxygen and Carbon Dioxide Plasmas in the Vacuum Ultraviolet Region," *Journal of Quantitative Spectroscopy and Radiative Transfer*, Vol. 20, 1978, pp. 175–189.

[45]Bauschlicher, C. W. and Langhoff, S. R., "Theoretical Study of the First and Second Negative System of N_2^+," *Journal of Chemical Physics*, Vol. 88, No. 1, 1988, pp. 329–338.

[46]Laux, C. O. and Kruger, C. H., "Arrays of Radiative Transition Probabilities for the N_2 First and Second Positive, NO Beta and Gamma N_2^+ First Negative, and O_2 Schumann-Runge Band Systems," *Journal of Quantitative Spectroscopy and Radiative Transfer*, Vol. 48, No. 1, 1992, pp. 9–24.

[47]Stark, G., Huber, K. P., Yoshino, K., Chan, M.-C., Matsui, T., Smith, P. L., and Ito, K., "Line Oscillator Strength Measurements in the 0-0 Band of the c4 1S+u – X1Sg+ Transition of N2," *The Astrophysical Journal*, Vol. 531, 2000, pp. 321–328.

[48]Chan, W. F., Cooper, G., Sodhi, R. N. S., and Brion, C. E., "Absolute Optical Oscillator Strengths for Discrete and Continuum Photoabsorption of Molecular Nitrogen (11-200 eV)," *Chemical Physics*, Vol. 170, 1993, pp. 81–97.

[49]Appleton, J. P. and Steinberg, M., "Vacuum-Ultraviolet Absorption of Shock-Heated Vibrationally Excited Nitrogen," *Chemical Physics*, Vol. 46, No. 4, 1967, pp. 1521–1529.

[50]Carter, V. L., "High-Resolution N_2 Absorption Study from 730 to 980 A," *Chemical Physics*, Vol. 56, No. 8, 1972, pp. 4195–4205.

[51]Allen, C. W., *Astrophysical Quantities*, London, 1962.

[52]Gryzinski, M., "Classical Theory of Electronic and Ionic Inelastic Collisions," *Physical Review*, Vol. 115, 1959, pp. 374–383.

[53]Frost, R. M., "Calculated Cross Sections and Measured Rate Coefficients for Electron-Impact Excitation of Neutral and Singly Ionized Nitrogen," *Journal of Applied Physics*, Vol. 84, 1998, pp. 2989–3003.

[54]Park, C., "Comparison of Electron and Electronic Temperatures in a Recombining Nozzle Flow of Ionized Nitrogen Hydrogen Mixture. Part 1. Theory," *Journal of Plasma Physics*, Vol. 9, 1973, pp. 187–215.

[55]Gorelov, V. A., "Experimental and Numerical Study of Nonequilibrium Ultraviolet NO and N_2^+ Emission in a Shock-Layer," *Journal of Thermophysics and Heat Transfer*, Vol. 12, 1998, pp. 172–179.

[56]Teulet, P., Sarrette, J. P., and Gomes, A. M., "Calculation of Electron-Impact Inelastic Cross-Sections and Rate Coefficients for Diatomic Molecules. Application to Air Molecules," *Journal of Quantitative Spectroscopy and Radiative Transfer*, Vol. 62, 1999, pp. 549–569.

[57]Nagy, O., "Excitation Cross-Sections of N_2^+ Molecular Ion by Electron Impact and the Vibrational Energy Levels of the Three Target States," *Chemical Physics*, Vol. 286, 2003, pp. 109–114.

[58]Kleb, B., Thompson, R., and Johnston, C. O., "Blurring the Inputs: A Natural Language Approach to Sensitivity Analysis," AIAA Paper 2007–4206, June 2007.

American Institute of Aeronautics and Astronautics

[59]de Moivre, A., *The Doctrine of Chances: A Method of Calculating the Probabilities of Events in Play*, Millar, 2nd ed., 1738.

[60]Vose, D. R., *Risk Analsysis: A Quantitative Guide*, Wiley, 2nd ed., 2000.

[61]Cullen, A. C. and Frey, H. C., *Probabilitistic Techniques in Exposure Assessment: A Handbook for Dealing with Variability and Uncertainty in Models and Inputs*, Plenum Press, 1999.

[62]Kreinovich, V., Beck, J., Ferregut, C., Sanchez, A., Miller, G. R., Averill, M., and Starks, S. A., "Monte-Carlos-Type Techniques for Processing Interval Uncertainty, and Their Potential Engineering Applications," *Reliable Computing*, Vol. 13, 2007, pp. 25–69.

[63]Kreinovich, V. and Ferson, S. A., "A New Cauchy-Based Black-Box Technique for Uncertainty in Risk Analysis," *Reliability Engineering and Systems Safety*, Vol. 85, 2004, pp. 267–279.

[64]Gnoffo, P. A., "An Upwind-Biased, Point-Implicit Relaxation Algorithm for Viscous, Compressible Perfect-Gas Flows," NASA TP 2953, Feb. 1990.

[65]Gnoffo, P. A., Gupta, R. N., and Shinn, J. L., "Conservation Equaqtions and Physical Models for Hypersonic Air Flows in Thermal and Chemical Nonequilibrium," NASA TP 2867, Feb. 1989.

[66]Cauchon, D. L., "Radiative Heating Results from the Fire II Flight Experiment at a Reentry Velocity of 11.4 Kilometers Per Second," NASA TM X 1402, July 1967.